Author Manuscript

Author Manuscript

Author Manuscript

Author Manuscript

HHS Public Access

Author manuscript

J Biol Inorg Chem. Author manuscript; available in PMC 2020 December 01.

Published in final edited form as:

J Biol Inorg Chem. 2019 December ; 24(8): 1261–1268. doi:10.1007/s00775-019-01738-2.

Biometals as Conformational Modulators of α-Synuclein Photochemical Crosslinking

Dinendra L. Abeyawardhane, **Alyson M. Curry**, **Ashley K. Forney**, **Joel W. Roberts**, **Heather R. Lucas***

Department of Chemistry, Virginia Commonwealth University, Richmond VA 23284

Abstract

Metal dyshomeostasis has long been linked to Parkinson's disease (PD), and the amyloidogenic protein α-synuclein (αS) is universally recognized as a key player in PD pathology. Structural consequences upon coordination of copper and iron to αS have gained attention due to significant dyshomeostasis of both metals in the PD brain. Protein-metal association can navigate protein folding in distinctive pathways based on the identity of the bio-metal in question. In this work, we employed photo-chemical crosslinking of unmodified proteins (PICUP) to evaluate these potential metal ion induced structural alterations in the folding dynamics of N-terminally acetylated αS (^{NAc}αS) following metal coordination. Through fluorescence analysis and immunoblotting analyses following photoirradiation, we discovered that coordination of iron obstructs copper-promoted crosslinking. The absence of intra-molecular crosslinking upon iron association further supports its C-terminal coordination site and suggests a potential role for iron in mitigating nearby post-translational modification of tyrosine residues. Decreased fluorescence emission upon synergistic coordination of both copper and iron highlighted that although copper acts as a conformational promotor of ^{NAc}αS crosslinking, iron inhibits analogous conformational changes within the protein. The metal coordination preferences of ^{NAc}αS suggest that both competitive binding sites as well as dual metal coordination contribute to the changes in folding dynamics, unveiling unique structural orientations for ^{NAc}αS that have a direct and measureable influence on photoinitiated dityrosine crosslinks. Moreover, our findings have physiological implications in that iron overload, as is associated with PD-insulted brain tissue, may serve as a conformational block of copper-promoted protein oxidation.

Keywords

α-Synuclein; dityrosine; photochemical crosslinking; iron; copper

Introduction

Accumulation of misfolded α-synuclein (αS) protein and metal dyshomeostasis in the *substantia nigra pars compacta* (SNpc) have suggested the intertwined role of both of these pathogenic phenomena in the progression of Parkinson's disease (PD), an age-related neurodegenerative disorder.[1–4] The structural dynamics of this presynaptic protein upon

* hrlucas@vcu.edu.

Author Manuscript Author Manuscript Author Manuscript Author Manuscript

interaction with biometals has been suggested to vary depending on the metal bound.[5] Evidence for depletion of copper and accumulation of iron in the SNpc upon aging and among PD victims further inspired various studies to be focused on αS protein behavior upon encountering the aforementioned metals.[6]

Although the metal-mediated aggregation properties of non-acetylated αS have been extensively studied over the past decade, N-terminally acetylated αS (^{NAc}αS), the native form in humans, lacked attention up until recently.[7, 8] Therefore, our group in particular analyzed the structural dynamics of ^{NAc}αS upon coordination to Cu^{I} and Fe^{II}.[9, 10] Strikingly different conformational changes were observed with both metals in which Fe^{II}-O_2 chemistry promoted an oligomer-locked right twisted β-sheet structure as opposed to the fibrillar formation which was favored upon Cu^{I} interaction. The structural consequences of redox-active metal-bound protein were characterized upon exposure to atmospheric oxygen in order to simulate cellular mechanisms in the reducing environment of living cells under oxidative stress. Aggregation of aerobic copper-bound ^{NAc}αS resulted in dityrosine crosslinks,[9] a common post translational modification (PTM) found in the post-mortem analysis of PD brains, while aerobic iron-bound ^{NAc}αS resulted in Schiff base formation.[10] The dissimilar PTMs induced by these distinct biometals during ^{NAc}αS aggregation underpin the unique reaction pathways promoted by metal-bound ^{NAc}αS and suggest coordination site modulation of the global protein dynamics.

In order to evaluate the earliest stages of metal-induced changes in ^{NAc}αS protein structure, photo-initiated crosslinking was employed following iron and copper protein coordination. Our previous studies imply that metal interaction with monomeric ^{NAc}αS initiates structural changes that lead to disparities upon aggregation. Crosslinking of amyloidogenic proteins has been deployed to monitor oligomer populations and assembly. The metastable nature of amyloidogenic protein conformers, which are relevant to numerous neurodegenerative diseases, can be circumvented by induction of crosslinks via chemical or photochemical methods.[11–14] Analysis of protein interactions by chemical crosslinking is typically mediated by bifunctional crosslinkers connected by a linker arm; however, poor yields and lack of controllability of the reaction have limited its application. Photochemical activation of crosslinking is rapid and higher in yield. Irradiation at a visible light range as opposed to UV light can further be beneficial in physiological applications, as most subcellular components and organelles are prone to damage by UV light. We utilized the PICUP (photo-induced crosslinking of unmodified proteins) technique (Fig. 1) developed by the Kodadek group to shed light on the dynamic conformational response of ^{NAc}αS upon coordination of iron and copper.[15] Although protein behavior may vary at different stages of the aggregation process, chemical photo-induction facilitates the immediate crosslinking of proteins; therefore it is a powerful tool to complement extended aggregation experiments when investigating the role of biometal coordination in protein interactions and structural modifications.

The PICUP catalytic cycle (Fig. 1) utilizes tris(bipyridine)ruthenium(II) ($[Ru(bpy)_3]^{2+}$) as a photosensitizer and ammonium persulfate (APS) as an electron acceptor to facilitate catalyst turnover.[11, 16, 17] The process is initiated by excitation of $[Ru(bpy)_3]^{2+}$ at 450 nm (blue light), and the metal-to-ligand charge transfer results in an excited triplet state. The

Author Manuscript Author Manuscript Author Manuscript Author Manuscript

outcomes of an electron donation from this state to APS are $[Ru(bpy)_3]^{3+}$, sulfate radical, and sulfate anion. In the absence of APS, molecular oxygen acts as a quencher of the excited $[Ru(bpy)_3]^{2+}$ state, although it is inefficient and thus the yield of protein crosslinking is significantly decreased in these cases.[18] Both $[Ru(bpy)_3]^{3+}$ and sulfate radical can act as one-electron oxidants, and amino acid residues like tyrosine, tryptophan, and cysteine are potent candidates. Due to lack of tryptophan and cysteine in the native sequence of $^{NAc}\alpha S$, tyrosine is the main residue targeted for oxidation. Thus, tyrosyl radical formation by hydrogen atom abstraction propels covalent bond formation with a second tyrosyl radical to generate dityrosine, resulting in the intra- or inter-molecular bridging of protein molecules, depending on which tyrosine residues are involved. In $^{NAc}\alpha S$, tyrosine residues are positioned at 39, 125, 133, and 136 (Fig. 2), and the localized C-terminal distribution suggests that any turbulence in this region caused by metal binding could be monitored using the PICUP technique.

Dityrosine is a natural fluorophore with a distinctive emission at ~ 410 nm upon excitation at 320 nm, so the ensemble average of the dityrosine content of PICUP samples can be monitored spectroscopically.[16, 19] In parallel, dityrosine formation can be assessed by immunoblotting to gain insight on the distribution of inter-molecular and intra-molecular crosslinking. We deployed these techniques to reveal the structural consequences of metal binding on $^{NAc}\alpha S$, a key player in the progression of PD. Although PICUP has previously aided in characterization of amyloid-β and αS oligomerization patterns,[20–22] this study marks the first approach to monitor conformational changes of metal-coordinated amyloidogenic protein via photo-induction, a critical topic given the well-known link between metal dyshomeostasis and a host of neurodegenerative diseases.

Experimental Section

Materials.

Tris(bipyridine)ruthenium(II) chloride complex ($Ru(bpy)_3Cl_2$) was synthesized according to published procedures.[23] Trifluoromethanesulfonate salts of the metal ions were purchased from Sigma Aldrich, and all other reagents used were analytical grade and purchased from commercial sources. Construction and purification of $^{NAc}\alpha S$ were conducted in a manner consistent with a previously described procedure.[9, 10] The cotransformation construct, pNatB, was a gift from Dr. Daniel Mulvihill.[24]

Photoinduced crosslinking of $^{NAc}\alpha S$.

Flash frozen $^{NAc}\alpha S$ samples were thawed and exchanged into 20 mM 3-(N-morpholino)propanesulfonic acid (MOPS; GoldBio), 100 mM NaCl, pH 7.0 using a PD-10 desalting column. Protein solutions (35 μM) were supplemented with stoichiometric ratios of metal ions. For competitive studies, iron ions were added first followed by immediate addition of copper ions. The stock solutions of tris(bipyridine)ruthenium(II) chloride complex ($Ru(bpy)_3Cl_2$) and ammonium persulfate (APS) were prepared in deionized water. The concentration of $Ru(bpy)_3Cl_2$ was maintained at 10 μM in the protein-metal sample and APS was added in a 20-fold molar excess (200 μM). Addition of $Ru(bpy)_3Cl_2$ and APS was

Author Manuscript Author Manuscript Author Manuscript Author Manuscript

conducted under dark conditions and samples were irradiated for 20 minutes using a Micro Photochemical Reactor (Aldrich) equipped with blue LED lights.

Protein Analysis Following PICUP.

After irradiation, the dityrosine fluorescence emission of each sample was recorded from 340 nm to 520 nm upon excitation at 320 nm using an F-4500 fluorescence spectrophotometer (Hitachi). For SDS gel electrophoresis and Western blotting, sample aliquots were diluted in 1x SDS gel loading buffer and dithiothreitol (DTT). The samples were heated to 95 °C for 5 min, and loaded to 4-20% precast polyacrylamide gels (ClearPage, CBS Scientific). Visualization was conducted using Coomassie blue stain. For western blotting, the separated bands were transferred to 0.2 micron nitrocellulose membrane using an iBlot 2 Dry Blotting System (Thermo Fisher Scientific). The SNAP i.d. 2.0 protein detection system (Millipore Sigma) was used for further steps such as blocking, antibody incubation, and washing. The blocking step was conducted using SuperBlock (PBS) blocking buffer (Thermo Fisher Scientific) containing 0.1% Tween 20. The blot was probed with mouse anti-dityrosine (1:250) monoclonal antibody (JaICA, Japan) and SuperSignal Western Blot Enhancer (Thermo Fisher Scientific) was used at room temperature for 20 minutes. The blot was washed with PBS-T (0.1 M Na_2HPO_4, 0.15 M NaCl, pH 7.2, and 0.1% Tween-20) for three times, and incubated with goat anti-mouse IgG (H+L) HRP (1:500) secondary antibody (Thermo Fisher Scientific) in 10% SuperBlock Blocking buffer containing 0.1% Tween-20 at room temperature for 20 minutes. The blot was washed again three times with PBS-T and two times with PBS. Colorimetric development was applied to the blot using 1-step TMB blotting solution (Thermo Fisher Scientific), and the reaction was ceased by rinsing with water.

Results and Discussion

Photo-initiated crosslinking of ^{NAc}αS has been investigated in order to examine the contribution of bound metal to the structural dynamics of the protein. Copper and iron were specifically selected due to PD relevance. We had previously demonstrated that aggregation of ^{NAc}αS during metal exposure resulted in covalent intermolecular (Y39-Y39) and intramolecular (C-terminal) dityrosine linkages only in samples supplemented with stoichiometric copper, likely mediated by a protein-bound Cu-superoxide intermediate.[9] Dityrosine crosslinks were not observed in aggregated Fe-bound ^{NAc}αS samples. It has been previously reported that Fe^{II} binding to ^{NAc}αS favors the C-terminus, putatively around Asp121.[25, 26] The majority of ^{NAc}αS tyrosine residues are located around this region, which may result in iron having an effect on the photo-initiated crosslinking process. Although it has not been fully elucidated, it has been postulated that iron also interacts with ^{NAc}αS at or near the His50 site, which could also affect Tyr39 crosslinking.[2] Herein, we discuss consequences of protein conformational changes that are steered by metal coordination. The rapid photo-crosslinking technique PICUP has been utilized to highlight the global changes in tyrosine radical coupling upon metal coordination, shedding light on metal-mediated dynamics of ^{NAc}αS.

Author Manuscript Author Manuscript Author Manuscript Author Manuscript

Photo-crosslinking with iron vs copper

The monomeric protein was supplemented with stoichiometric levels of metal (35 μM) and photo-initiated at 450 nm for 20 minutes upon addition of 10 μM $Ru(bpy)_3Cl_2$ and 20-fold APS. A control sample of $^{NAc}\alpha S$ without metal added was analyzed in parallel to metal-supplemented samples in order to evaluate the change in protein dynamics upon coordination to the aforementioned metal ions. Immunoblotting analysis against the monoclonal dityrosine antibody (clone, IC3) revealed the presence of inter-molecular dityrosine crosslinks in all samples, with the copper-bound samples having measurably higher levels (Fig. 3). The iron-bound samples have a slightly reduced dityrosine signal relative to the no-metal-added control. This result implies that iron coordination at the C-terminus or at His50 may hinder dityrosine formation by (i) disfavoring conformations where tyrosine residues are oriented correctly for coupling or (ii) directly blocking physical access to tyrosine side chains. Notably, both monomeric and dimeric signals were observed in the Western blot of copper-coordinated $^{NAc}\alpha S$ samples for both redox states of copper, indicating the presence of both intra- and inter-molecular dityrosine crosslinking in these samples. Intra-molecular crossklinking was not observed in the no-metal control reaction nor in the PICUP samples supplemented with Fe in either redox state.

In order to address any fluorescence emission initiated by PICUP components and metal ions in the same region as dityrosine emission, control experiments were conducted without $[Ru(bpy)_3]Cl_2$ or APS. As expected, samples lacking photosensitizer demonstrated no dityrosine signal upon photo-irradiation. However, weak fluorescence signals were detected for all the samples upon exclusion of APS from the system. It has been previously confirmed that the excited $[Ru(bpy)_3]^{2+}$ state can be quenched by molecular oxygen due to its electron accepting properties.[18] Although drastically reduced, the differential metal coordination influenced the formation of dityrosine even under these conditions (Fig S1). None of the samples reported in this study have depicted a characteristic dityrosine emission prior to exposure of the blue light.

Fe^{II} as a structural modifier

Copper and iron may compete for overlapping binding sites in $^{NAc}\alpha S$, since both are known to have affinity for the acidic C-terminal region and both have been postulated to interact with His 50, the only histidine in $^{NAc}\alpha S$.[2, 27] Accordingly, we probed the impact that each metal might have on the other in the context of $^{NAc}\alpha S$ structural dynamics by conducting PICUP experiments in the presence of two metals.

In the case of $^{NAc}\alpha S$ supplemented with both Fe^{II} and Cu^{I}, where both metals are in the reduced redox state, the presence of Fe^{II} results in a decrease in the overall fluorescence signal relative to that of Cu^{I} alone (Fig. 4A). Moreover, the corresponding immunoblotting data (Fig. 4B) reveal that in the presence of Fe^{II}, the intra-molecular crosslinking specific to copper is diminished. These data suggest that Fe^{II} is successfully competing with Cu^{I} for binding sites near tyrosine residues, likely at the C-terminus based on the weighted distribution of tyrosine residues at that location. Indeed, Fe^{II} demonstrates similar trends in the interference of Cu^{II} PICUP reactions, resulting in a dramatically lower fluorescence signal (Fig. 4C) and a decreased level of intramolecular crosslinking as shown on the

Author Manuscript Author Manuscript Author Manuscript Author Manuscript

Western blot (Fig. 4D). A 20% reduction in the dityrosine fluorescence intensity at 410 nm for the corresponding $^{NAc}\alpha S$-Fe^{II} implicated the binding of the metal ion around the same region where intra-molecular dityrosine crosslinking can be initiated in the copper-bound samples (Fig 4C). Absence of intra-molecular crosslinks in the complementary immunoblot analysis supported the inhibition of intra-molecular tyrosine radical coupling due to steric hindrance upon Fe coordination (Fig 4D).

Evaluation of integrated fluorescence signals of copper-coordinated protein noted an ~ 43% enhancement for $^{NAc}\alpha S$-Cu^{II} in comparison to the effect of Cu^{I} (Fig 5), implying a potent role in the binding site of each oxidation state. Based on EPR characterization and Peisach-Blumberg structural correlation, we established that Cu^{II} coordination to $^{NAc}\alpha S$ adheres to an N3O1 binding mode involving the His50 imidazole and backbone nitrogen, the Val49 backbone nitrogen, and the oxygen donor from a water molecule.[27] Also, a secondary binding site was resolved from EPR hyperfine splitting patterns that involves an oxygen donor from Asp121 replacing the water molecule. Hence, this interaction can change the global peptide arrangement and stabilize the two termini at a closer proximity. Moreover, it allows the tyrosine residues located at the C-terminus to easily access the tyrosine at the N-terminus. Precursory computational calculations of Cu^{II} binding sites of αS also support these binding site locations.[28] It has been well established that copper promotes tyrosine radical formation in amyloidogenic proteins such as amyloid-β and αS, which eventually results in dityrosine crosslinking post-aggregation,[9, 29, 30] and our data presented herein suggest that copper-bound $^{NAc}\alpha S$ may modulate the protein in an orientation that favors dimeric and/or intramolecular coupling.

Photoirradiation unveils the role of bio-metals in guiding protein folding mechanisms based on the differing trends detected for the crosslinking of tyrosine. The presence of both Fe^{II} and Cu^{II} may involve competitive coordination of either species around the C-terminal site. Addition of Fe^{II} prior to Cu^{II} may favor iron binding at the respective site, whereas Cu^{II} can adapt to an alternative binding mode. Brown and coworkers have postulated that bimetallic coordination facilitates αS ferrireductase activity.[31] Even though $^{NAc}\alpha S$-Fe^{II} lacks intra-molecular crosslinks, Fe^{II} and Cu^{II} dual-coordinated protein depicts both intra- and inter-molecular crosslinks. In fact, the intra-molecular dityrosine crosslinking of dual metal-bound $^{NAc}\alpha S$ samples was reduced by 60% in comparison to $^{NAc}\alpha S$-Cu^{II} and the corresponding fluorescence signal was significantly decreased by ~ 63% (** $p < 0.01$) as depicted in Fig 5. Since both metals are added in sequence and may have similar coordination sites, 100% efficiency of Fe^{II} coordination might not be plausible under the experimental conditions due to competitive binding at the C-terminus.

On the contrary, binding of Cu^{I} is constrained at the N-terminus near the N-acetylation site of αS.[32] The coordination sphere of Cu^{I} is confined to Met1 and Met5 at the N-terminus. Based on NMR spectroscopy, Fernández and co-workers have also established another low-affinity site for Cu^{I} coordination comprising Met116 and Met127.[32] It is possible that binding of Cu^{I} at this site may lead to some hindrance for tyrosine at the C-terminus (mainly Tyr125) to interact with other tyrosine residues. Hence, the 30% decrease in dityrosine fluorescence emission of $^{NAc}\alpha S$-Cu^{I} as opposed to Cu^{II}-associated protein may be due to this secondary site (Fig 5). It is, however, most likely that Cu^{I} binding within the first five

Author Manuscript Author Manuscript Author Manuscript Author Manuscript

residues of $^{NAc}\alpha S$ has downstream consequences on the protein orientation that diminishes dityrosine formation. The statistical significance of decline in fluorescence was higher for $^{NAc}\alpha S$-Cu^{II} versus $^{NAc}\alpha S$-Fe^{II} (**$p < 0.01$) when compared to analogous trends demonstrated for $^{NAc}\alpha S$-Cu^{I} versus $^{NAc}\alpha S$-Fe^{II} (*$p < 0.05$). Moreover, addition of Fe^{II} followed by Cu^{I} indicated a moderate 20% decrease in emission signal relative to $^{NAc}\alpha S$-Cu^{I} alone, yet a 38% increase in the signal relative to $^{NAc}\alpha S$-Fe^{II} alone. This could be rationalized by differential coordination of both metals at opposite termini, which potentially reinforces orthogonal modulatory effects on protein crosslinking.

Role of different oxidation states of iron

We also evaluated the effect of Fe^{III} on dityrosine formation following photo-irradiation. Similar to $^{NAc}\alpha S$-Fe^{II}, Fe^{III} coordination inhibited intra-molecular crosslinking (Fig 6) due to structural limitations enforced by iron interaction at the C-terminus. However, there was an ~10% enhancement in dityrosine fluorescence as compared to the control ($^{NAc}\alpha S$ without any metal). Higher order oligomers such as trimers and tetramers in addition to dimers were detected for $^{NAc}\alpha S$-Fe^{III} following PICUP based on the Western blot, which would collectively contribute to the enhanced fluorescence signal. Although the coordination site of Fe^{III} in $^{NAc}\alpha S$ has not been fully characterized, it is believed to be in the C-terminal region like Fe^{II}. Supplementation of copper ions (Cu^{I} or Cu^{II}) alongside Fe^{III} resulted in a substantial decrease in fluorescence emission in comparison to copper alone (Fig 6). In fact, the most significant loss of dityrosine signal (50%) was demonstrated for Fe^{III}+Cu^{II} versus Cu^{II} alone (**$p < 0.01$). Notably, the corresponding Western blot analysis revealed an ~ 50% decrease in total dityrosine crosslinks, complementing the reduction in fluorescence. In comparison to Fe^{III} alone, augmented polymerization was detected in the form of multiple higher order bands for dual Fe^{III} and copper supplemented samples on the immunoblot. Our results pinpoint the crucial influence of C-terminal metal coordination to modulate the protein folding dynamics. Theoretically, preferential metal binding at the C-terminus is supported by an electrostatic shielding effect ensued upon neutralization of negatively charged residues.[33]

Conclusion

Photo-induced crosslinking of unmodified proteins is a strategic approach to trap metastable protein intermediates through the triggered generation of covalent linkages, providing a glimpse at the early dynamics of $^{NAc}\alpha S$ protein-protein interactions influenced by metal cofactors and their redox states, as occurs upon coordination of copper and iron. Notably, PICUP has not been previously employed to evaluate structural consequences of proteins following metal coordination; thus, this study marks a novel application of this well-established technique. In our work, we demonstrate that copper association structurally favors tyrosyl radical coupling while coordination of iron mitigates protein folding pathways that promote dityrosine crosslinking. No intra-molecular dityrosine crosslinking was detected upon coordination of iron at the C-terminus, likely due to the proximity of tyrosine residues. The principal binding sites of both copper redox states are in different regions than the iron coordination site; therefore, copper-mediated crosslinking outcompetes and/or preserves intra-molecular interactions despite the presence of iron in the system. Overall, our

Author Manuscript Author Manuscript Author Manuscript Author Manuscript

results underpin the importance of biometals in modulating the structural orientation of proteins, which may aid in the understanding of disease pathology and/or native biophysical dynamics. Moreover, the development of sensitive tools to understand the contribution of biometal-mediated molecular mechanisms driving PTM formation may have applications in PD biomarker discovery.

Supplementary Material

Refer to Web version on PubMed Central for supplementary material.

Acknowledgements

Research reported in this publication was supported by NIH R01 GM134015, the National Center for Advancing Translational Sciences Clinical and Translational Science Award (UL1TR002649), and the Center for Clinical and Translational Research Endowment Fund of Virginia Commonwealth University, as well as by the VCU College of Humanities and Sciences. We would also like to express our appreciation to the United States Secret Service for donation of the Hitachi F-4500 fluorescence spectrophotometer and Hitachi U-3310 UV/vis spectrophotometer to the Lucas lab.

References

1. Lashuel H, Overk C, Oueslati A and Masliah E (2013) Nature Reviews Neuroscience 14:38–48 [PubMed: 23254192]
2. González N, Arcos-López T, König A, Quintanar L, Menacho Márquez M, Outeiro TF and Fernández CO (2019) Journal of Neurochemistry 150:507–521 [PubMed: 31099098]
3. Joppe K, Roser A-E, Maass F and Lingor P (2019) Frontiers in Neuroscience 13:15 [PubMed: 30723395]
4. Abeyawardhane DL and Lucas HR (2019) Oxidative Medicine and Cellular Longevity
5. Theillet F, Binolfi A, Bekei B, Martorana A, Rose H, Stuiver M, Verzini S, Lorenz D, van Rossum M, Goldfarb D and Selenko P (2016) Nature 530:45-+ [PubMed: 26808899]
6. Davies KM, Bohic S, Carmona A, Ortega R, Cottam V, Hare DJ, Finberg JP, Reyes S, Halliday GM, Mercer JF and Double KL (2014) Neurobiol Aging 35:858–866 [PubMed: 24176624]
7. Moriarty GM, Janowska MK, Kang L and Baum J (2013) FEBS Lett 587:1128–1138 [PubMed: 23499431]
8. Lucas HR and Fernández RD (2019) Neural Regener Res
9. Abeyawardhane DL, Fernández RD, Heitger DR, Crozier MK, Wolver JC and Lucas HR (2018) J Am Chem Soc 140:17086–17094 [PubMed: 30422655]
10. Abeyawardhane DL, Fernández RD, Murgas CJ, Heitger DR, Forney AK, Crozier MK and Lucas HR (2018) J Am Chem Soc 140:5028–5032 [PubMed: 29608844]
11. Preston GW and Wilson AJ (2013) Chem Soc Rev 42:3289–3301 [PubMed: 23396550]
12. Houée-Lévin C, Bobrowski K, Horakova L, Karademir B, Schöneich C, Davies MJ and Spickett CM (2015) Free Radic Res 49:347–373 [PubMed: 25812585]
13. Fernández RD and Lucas HR (2018) Protein Expression and Purification 152:146–154 [PubMed: 30041032]
14. Dettmer U, Newman AJ, Luth ES, Bartels T and Selkoe D (2013) J Biol Chem 288:6371–6385 [PubMed: 23319586]
15. Fancy DA and Kodadek T (1999) Proc Natl Acad Sci U S A 96:6020–6024 [PubMed: 10339534]
16. Borsarelli CD, Falomir-Lockhart LJ, Ostatná V, Fauerbach JA, Hsiao H-H, Urlaub H, Paleček E, Jares-Erijman EA and Jovin TM (2012) Free Radical Biology and Medicine 53:1004–1015 [PubMed: 22771470]
17. Fancy DA, Denison C, Kim K, Xie Y, Holdeman T, Amini F and Kodadek T (2000) Chemistry & Biology 7:697–708 [PubMed: 10980450]

Author Manuscript Author Manuscript Author Manuscript Author Manuscript

18. Andreev OA, Reshetnyak YK and Goldfarb RH (2002) Photochem Photobiol Sci 1:834–836 [PubMed: 12656487]
19. DiMarco T and Giulivi C (2007) Mass Spectrom Rev 26:108–120 [PubMed: 17019703]
20. Rahimi F, Maiti P and Bitan G (2009) J Vis Exp
21. Bitan G, Lomakin A and Teplow DB (2001) J Biol Chem 276:35176–35184 [PubMed: 11441003]
22. Lopes DHJ, Sinha S, Rosensweig C and Bitan G (2012) In: Sigurdsson EM, Calero M and Gasset M (eds) Amyloid proteins: Methods and protocols. Humana Press, Totowa, NJ, pp. 11–21
23. Sullivan BP, Salmon DJ and Meyer TJ (1978) Inorganic Chemistry 17:3334–3341
24. Johnson M, Coulton AT, Geeves MA and Mulvihill DP (2010) PLoS One 5:e15801 [PubMed: 21203426]
25. Binolfi A, Rasia RM, Bertoncini CW, Ceolin M, Zweckstetter M, Griesinger C, Jovin TM and Fernández CO (2006) J Am Chem Soc 128:9893–9901 [PubMed: 16866548]
26. Peng Y, Wang C, Xu H, Liu Y and Zhou F (2010) Journal of Inorganic Biochemistry 104:365–370 [PubMed: 20005574]
27. Abeyawardhane DL, Heitger DR, Fernández RD, Forney AK and Lucas HR (2019) ACS Chemical Neuroscience 10:1402–1410 [PubMed: 30384594]
28. Ramis R, Ortega-Castro J, Vilanova B, Adrover M and Frau J (2017) J Phys Chem A 121:5711–5719 [PubMed: 28691818]
29. Al-Hilaly YK, Biasetti L, Blakeman BJ, Pollack SJ, Zibaee S, Abdul-Sada A, Thorpe JR, Xue WF and Serpell LC (2016) Sci Rep 6:39171 [PubMed: 27982082]
30. Atwood CS, Perry G, Zeng H, Kato Y, Jones WD, Ling KQ, Huang X, Moir RD, Wang D, Sayre LM, Smith MA, Chen SG and Bush AI (2004) Biochemistry 43:560–568 [PubMed: 14717612]
31. McDowall JS and Brown DR (2016) Metallomics 8:385–397 [PubMed: 26864076]
32. Miotto MC, Valiente-Gabioud AA, Rossetti G, Zweckstetter M, Carloni P, Selenko P, Griesinger C, Binolfi A and Fernández CO (2015) J Am Chem Soc 137:6444–6447 [PubMed: 25939020]
33. Bharathi, Indi S and Rao K (2007) Neuroscience Letters 424:78–82 [PubMed: 17714865]

Author Manuscript Author Manuscript Author Manuscript Author Manuscript

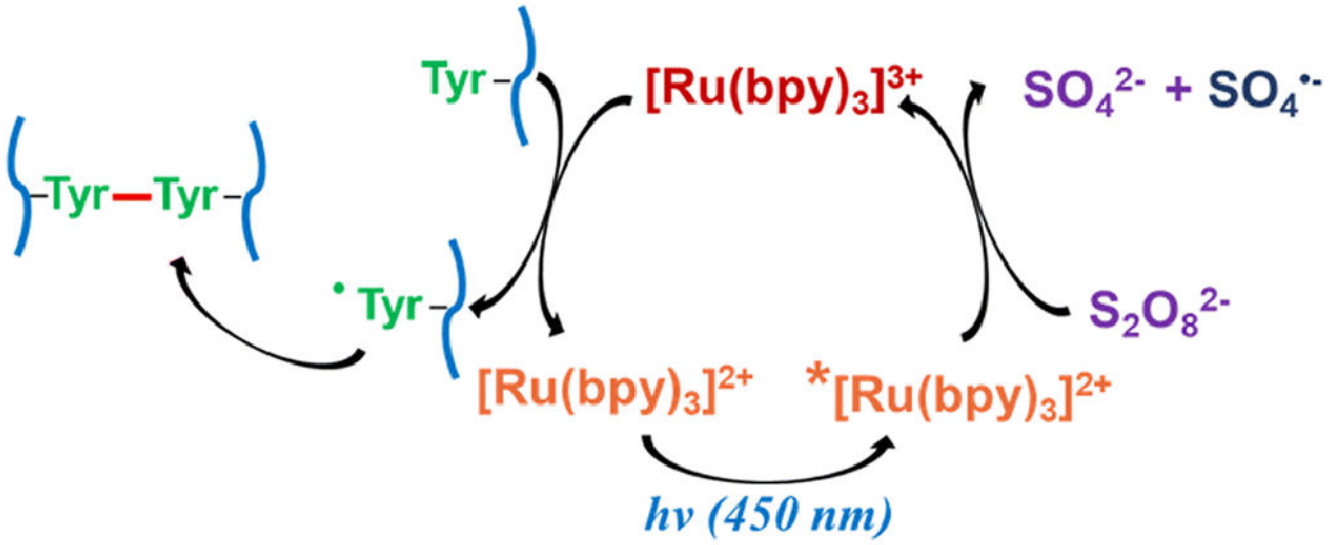

Fig 1.
Schematic representation of PICUP catalytic cycle

Author Manuscript Author Manuscript Author Manuscript Author Manuscript

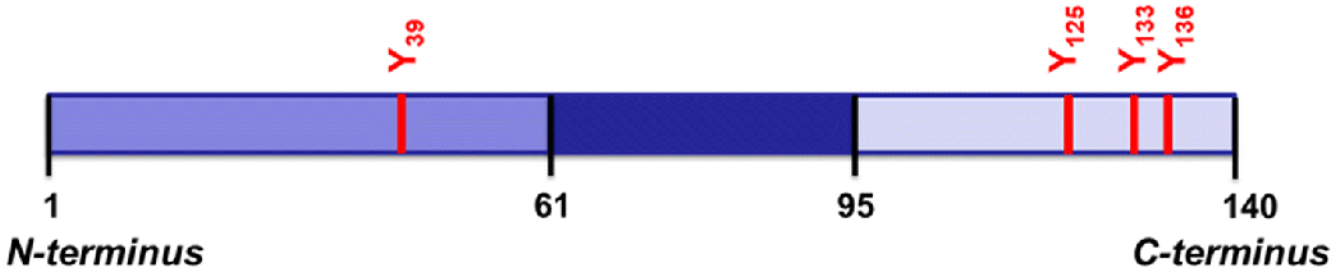

Fig 2.
Localization of tyrosine in the N-terminus and C-terminus of αS sequence.

Author Manuscript Author Manuscript Author Manuscript Author Manuscript

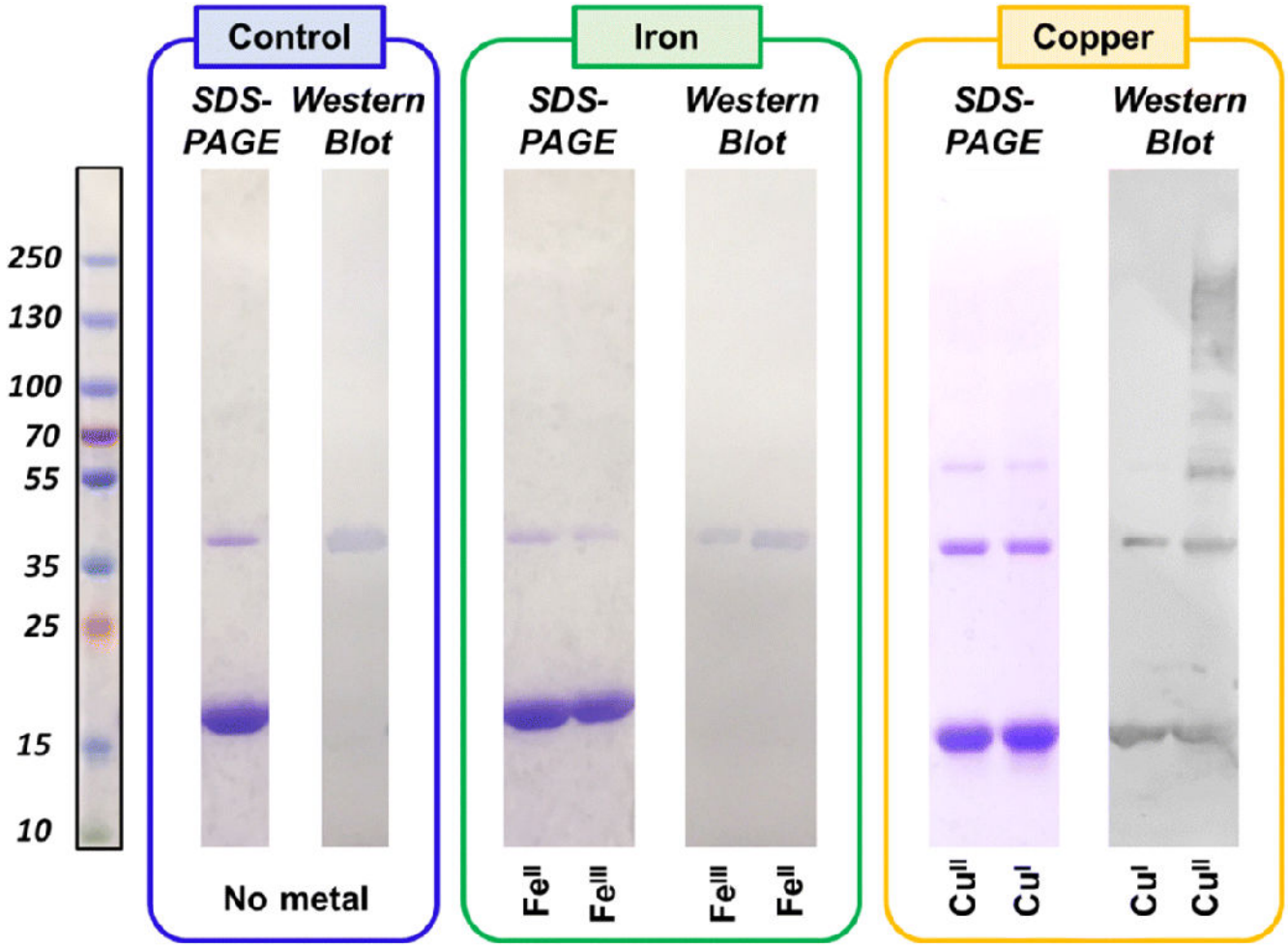

Fig 3.

SDS-PAGE gels and corresponding anti-dityrosine Western blot after photo-irradiation at 450 nm. $^{NAc}\alpha$S samples treated with stoichiometric ratios of Cu^{I}, Cu^{II}, Fe^{II}, and Fe^{III} are depicted along with no-metal-added control.

Author Manuscript Author Manuscript Author Manuscript Author Manuscript

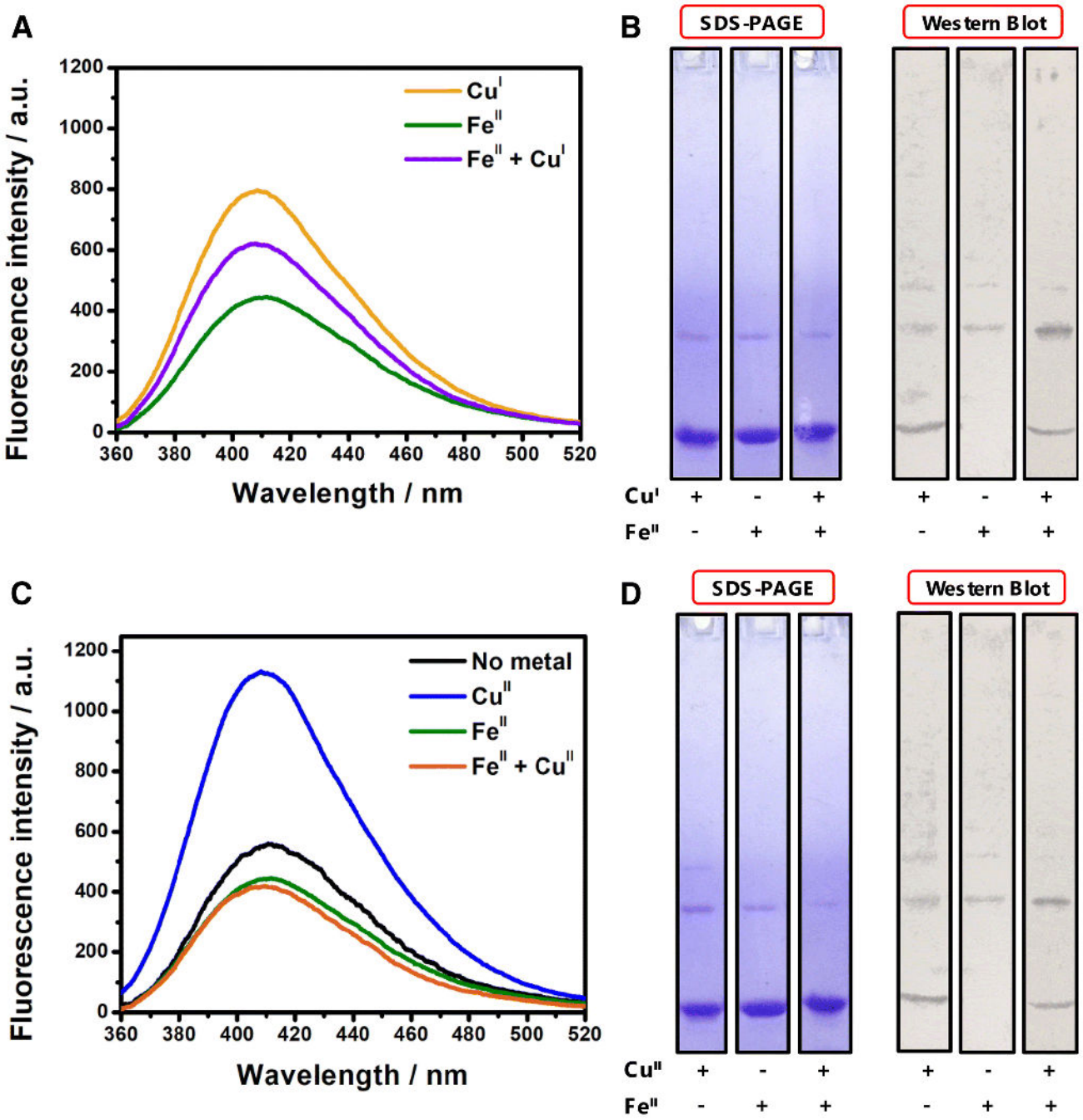

Fig 4.

A) Fluorescence spectra of PICUP samples corresponding to $^{NAc}\alpha S$-Cu^{I} (yellow), $^{NAc}\alpha S$-Fe^{II} (green), and $^{NAc}\alpha S$-Fe^{II} followed by immediate addition of Cu^{I} (purple). B) SDS-PAGE gel (left) and corresponding anti-dityrosine western blot (right) of PICUP samples of $^{NAc}\alpha S$ and metal combinations involving Cu^{I} and/or Fe^{II}. C) Fluorescence spectra of PICUP samples corresponding metal bound $^{NAc}\alpha S$; control $^{NAc}\alpha S$ in the absence of metals (black), $^{NAc}\alpha S$-Cu^{II} (blue), $^{NAc}\alpha S$-Fe^{II} (green), and $^{NAc}\alpha S$-Fe^{II} followed by immediate addition of

Author Manuscript Author Manuscript Author Manuscript Author Manuscript

Cu^{II} (orange). D) SDS-PAGE gel (left) and corresponding anti-dityrosine western blot (right) of PICUP samples of $^{NAc}\alpha S$ and metal combinations involving Cu^{II} and/or Fe^{II}.

Author Manuscript Author Manuscript Author Manuscript Author Manuscript

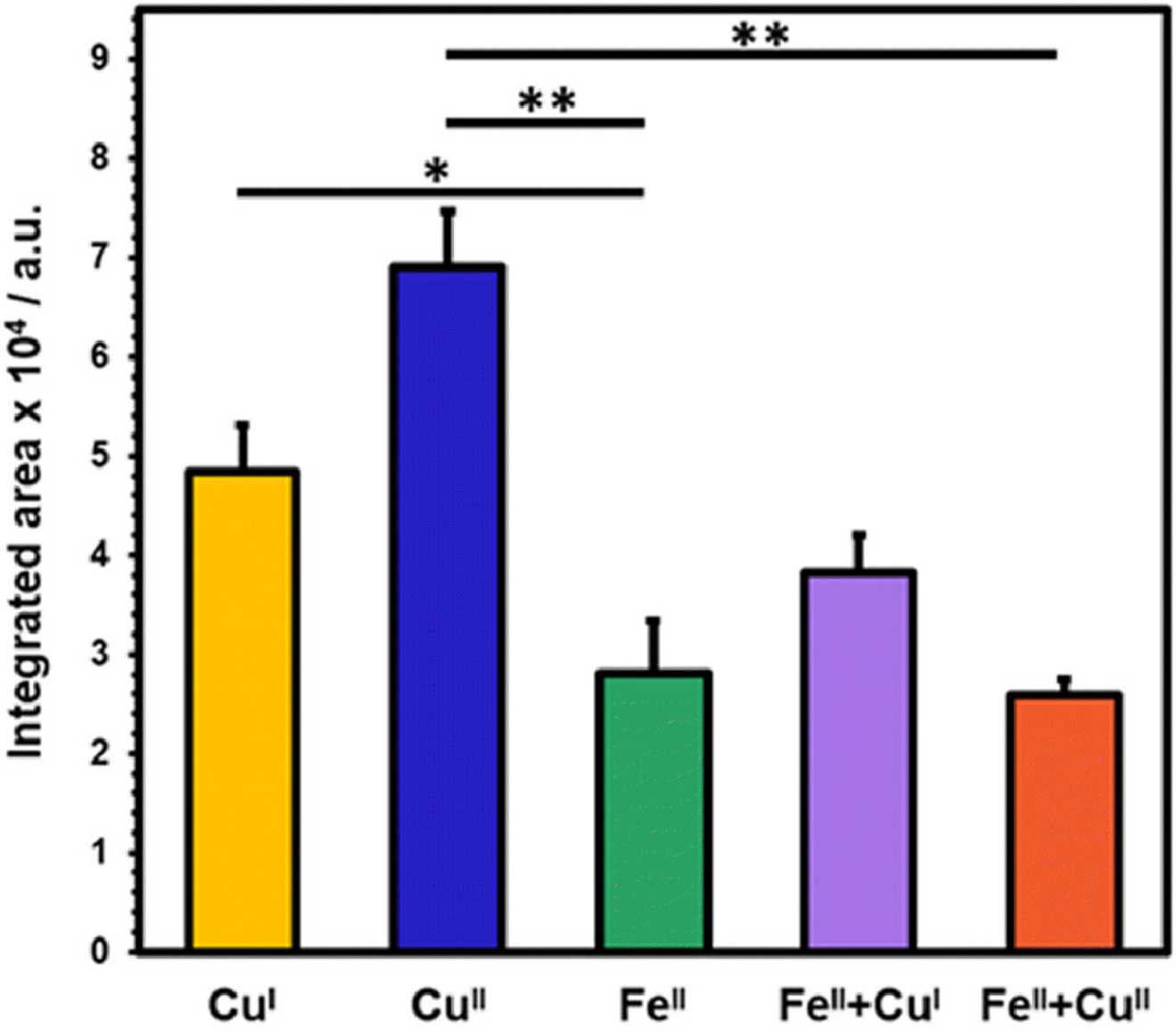

Fig 5.

A bar graph corresponding to fluorescence emission resulting from different metal combinations; ^{NAc}αS-Cu^{I} (yellow), ^{NAc}αS-Cu^{II} (blue), ^{NAc}αS-Fe^{II} (green), ^{NAc}αS-Fe^{II} followed by immediate addition of Cu^{I} (purple), and ^{NAc}αS-Fe^{II} followed by immediate addition of Cu^{II} (orange). The results are expressed as mean ± standard error. *$p < 0.05$, **$p < 0.01$.

Author Manuscript Author Manuscript Author Manuscript Author Manuscript

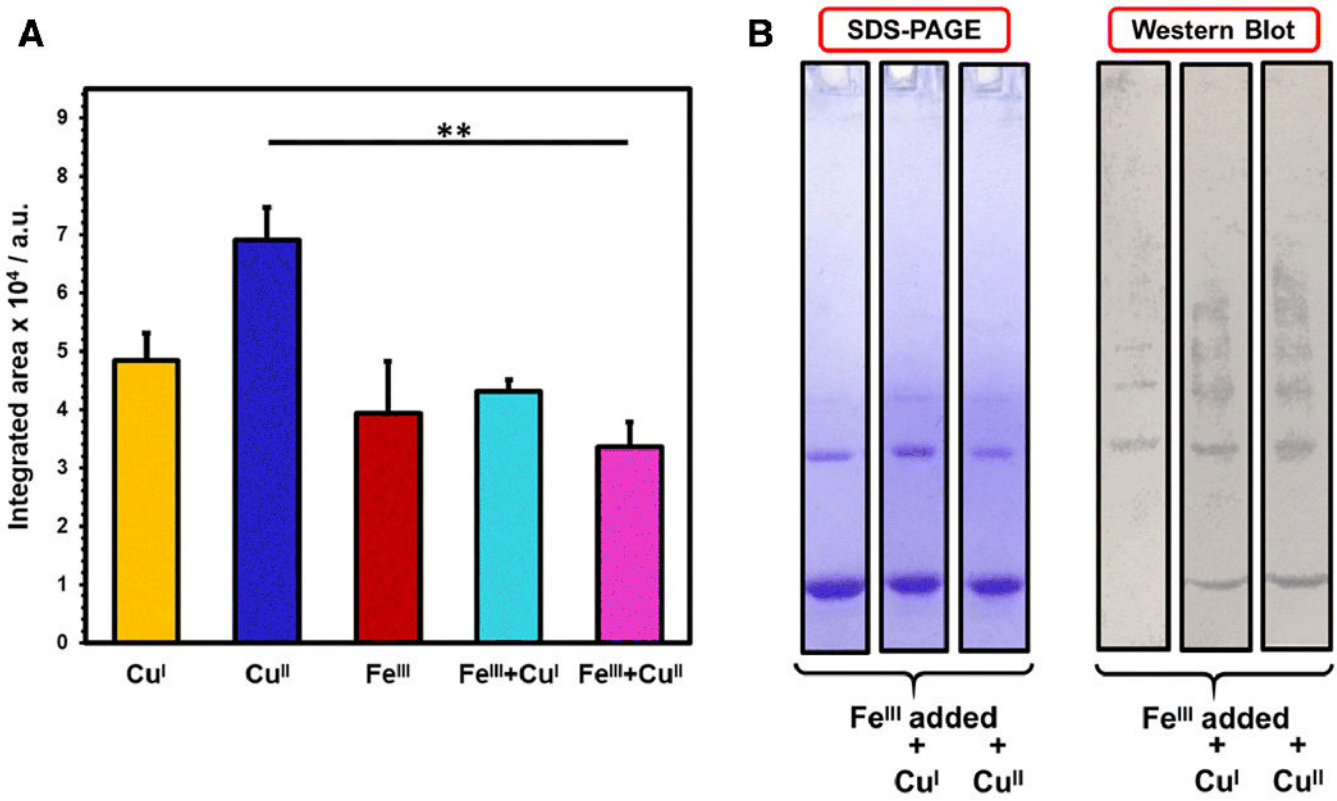

Fig 6.

Analysis of dityrosine crosslinks upon PICUP implementation on Fe^{III} supplemented $^{NAc}\alpha S$ samples. A) Bar graph corresponding to dityrosine fluorescence emission resulted from different metal combinations; $^{NAc}\alpha S$-Cu^{I} (yellow), $^{NAc}\alpha S$-Cu^{II} (blue), $^{NAc}\alpha S$-Fe^{III} (red), $^{NAc}\alpha S$-Fe^{III} followed by immediate addition of Cu^{I} (teal), and $^{NAc}\alpha S$-Fe^{III} followed by immediate addition of Cu^{II} (magenta). The results are expressed as mean ± standard error. $^{**}p < 0.01$. B) SDS-PAGE gel (left) and corresponding anti-dityrosine western blot (right) of $^{NAc}\alpha S$-Fe^{III} alone and metal combinations with Cu^{I} or Cu^{II}.